

# Supercomputer technologies in tomographic imaging applications

*Alexander V. Goncharsky*<sup>1</sup>, *Sergey Y. Romanov*<sup>1</sup>, *Sergey Y. Seryozhnikov*<sup>1</sup>

© The Authors 2017. This paper is published with open access at SuperFri.org

Currently, tomographic imaging is widely used in medical and industrial non-destructive testing applications. X-ray tomography is the prevalent imaging technology. Modern medical X-ray CT scanners provide up to 1 mm of spatial resolution. The disadvantage of X-ray tomography is that it cannot be used for regular medical examinations. Early breast cancer diagnosis is one of the most pressing issues in modern healthcare. Ultrasound tomography devices are being developed in the USA, Germany and Russia to address this problem. One of the main challenges in ultrasound tomographic imaging is the development of efficient algorithms for solving inverse problems of wave tomography, which are nonlinear three-dimensional coefficient inverse problems for a hyperbolic differential equation. Solving such computationally-expensive problems requires the use of supercomputers.

*Keywords: supercomputer, GPU cluster, wave-tomography imaging, coefficient inverse problems, scalar wave equation, breast cancer.*

## Introduction

Tomographic imaging methods are widely used in medicine, non-destructive testing in industry, microscopy, civil engineering, hydrolocation, and seismic studies [1-5]. In Greek, “tomography” means “slice”. Tomographic methods can significantly increase resolution for studying the internal structure of various objects. A typical example would be the comparison of the photofluorographic imaging methods and X-ray tomography. As you know, Röntgen had received his Nobel Prize at the beginning of the twentieth century for the discovery of X-rays. Almost immediately, X-ray examination was applied in medicine. Usually, one radiation source and one detector were used. The detector was a film sensitive to X-rays. Despite the high resolution of the film, resolving power remained low. At the end of this article, we will return to the concept of resolving power as the ability to distinguish fine details of the object.

Tomographic imaging suggests solving inverse problems. Surprisingly, mathematical foundations of computed tomography were developed at the same time, at the beginning of the twentieth century. The fundamental works in this area are studies in integral geometry (G. Minkovsky, 1905, P. Funk 1913, Y. Radon 1917). It took humankind half a century to invent first tomographs in the early 60s of the last century. This is primarily due to the fact that the tomographic methods cannot be implemented without using computers. The first tomographs were X-ray tomographs focused on medical research.

Modern X-ray tomographs are very complex machines, and solving mathematical problems is not the most difficult issue. From the mathematical point of view, the inverse problem of X-ray tomography is a linear operator equation that is reduced to two-dimensional integral equations that depend on the difference of the arguments. Solving such 2D problems numerically on a 1000×1000-point grid takes about few seconds using a regular personal computer. The use of graphics processing units (GPUs) allows performing complex image processing procedures, isolation of various internal structures, building 3D models, etc. [6, 7]. The volume of data used in modern X-ray tomography is about 1 GB, and the resolution of medical CT scanners is about 1 mm.

<sup>1</sup>Lomonosov Moscow State University, Moscow, Russia

In this article, the term “tomographic examination” is understood in a broad sense. It would be easier to formulate, what is not a tomographic examination in our understanding. Tomographic studies do not include the methods where one fixed detector and one fixed source are used. If the source and the detector change their position, then such examination may be considered tomographic, from the extended point of view. As a rule, in X-ray tomography the source and the detector run around the scanned object.

In some applications we cannot place sources and detectors around the object. For example, in Synthetic Aperture Radars (SAR), used for studying the surface of the Earth from the space or from an aircraft, sources and detectors may be positioned on a straight line, at a great distance from the examined object. However, such a measurement scheme provides amazing results and may be classified as a tomographic method. The synthetic aperture method allows increasing the image resolution up to hundreds of times. The problems of interpreting the data of such an experiment are inverse problems. It is solving the inverse problems, which makes it possible to obtain high resolution.

In this article, an attempt is made to assess the possibility to use supercomputer technologies for improving and developing new tomographic methods. One of the most promising medical diagnostic methods is a ultrasonic method. All the ultrasonic methods currently used in medicine are not tomographic. Development of ultrasound tomographic equipment at the model level is performed extensively in the United States, Germany, and Russia [1, 8–10]. One of the main problems in ultrasonic tomography is creating efficient methods for solving inverse problems of wave tomography. Unlike X-ray tomography, the inverse problems of wave tomography are nonlinear, and cannot be solved without using powerful supercomputers. Supercomputer technologies open new possibilities for designing wave-based tomography devices. This area is discussed in detail in the article. The developed wave tomography methods can be used for medical examinations, non-destructive testing in industry and for seismic studies as well. One of the most promising applications is developing medical ultrasonic tomography devices for differential diagnosis of breast cancer.

## 1. Linear tomographic models

### 1.1. Formulation and methods of solving inverse problems of X-ray tomography

X-ray tomography is one of the most used diagnostic technologies both in medicine and in non-destructive testing of industrial products. Resolution of modern medical tomographs reaches 1–2 mm; CT scanners with resolution of about 10  $\mu\text{m}$  have been developed for industrial diagnostics at the micro-level.

The mathematical models used in X-ray tomography are the models of geometric optics [11]. The layer-by-layer approach is used for imaging three-dimensional objects. A 3D object is examined in layers, where in each of the layers the X-ray the absorption coefficient  $f(x,y)$  is reconstructed as a two-dimensional function of Cartesian coordinates  $x, y$ . The possibility of solving inverse problems of X-ray tomography separately in each layer is associated with the unique properties of X-ray radiation, which is easy to absorb, but is very difficult to deflect from the straight line. The refractive index of any material differs from unity by not more than hundredths of percent for X-ray radiation. The inverse problems of X-ray tomography are therefore linear.

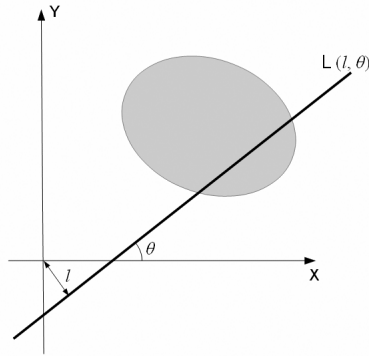


**Figure 1.** The scheme of X-ray tomography

Fig. 1 shows the scheme of X-ray tomography. The detectors measure the integral absorption along the lines  $L$  connecting each detector and a fixed source. Let us introduce a family of lines  $L(l, \theta)$  in the plane  $Oxy$ . The parameter  $l$  varies between  $-\infty$  and  $+\infty$ ,  $\theta$  varies between  $-\pi/2$  and  $\pi/2$ . If  $l$  and  $\theta$  can take all the values in the specified ranges, we call it a “full-range” tomography problem.

In reality, the studied object is usually compact, and it is sufficient to vary the parameter  $l$  in the specified limits. In the tomographic experiment, the integral absorption  $p(l, \theta)$  along the line  $L(l, \theta)$  is measured:

$$p(l, \theta) = \int_{L(l, \theta)} f(x, y) dl. \tag{1}$$

If the function  $f(x, y)$  is specified, calculation of  $p(l, \theta)$  by formula (1) is a forward problem described by the Radon transform [12]. The inverse problem of X-ray tomography may be formulated as a problem of solving an operator equation

$$Af = \int_{L(l, \theta)} f(x, y) dl = p(l, \theta). \tag{2}$$

For the sake of simplicity, we will consider a case where the functions  $f(x, y)$  and  $p(l, \theta)$  are square integrable. In this case, the operator  $A$  acts from the  $\mathbf{L}_2$  space of the square integrable functions into the same  $\mathbf{L}_2$  space. The inverse problem of X-ray tomography consists of finding a function  $f(x, y)$ , which is the solution of the equation (2), given a specified  $p(l, \theta)$ . The function  $p(l, \theta)$  is obtained from the experiment, therefore it is specified with some error  $\delta$ .

The distinctive feature of X-ray tomography problems is not only the linearity of the inverse problem (2), but the possibility of direct inversion of the operator  $A$  as well, i.e., the possibility of calculating the inverse operator  $A^{-1}$  in the domain of its definition  $D_A \subset \mathbf{L}_2$ . In the Hilbert space, the operator  $A$  has an adjoint operator  $A^*$ , which is determined by the relation  $(Af, p) = (f, A^*p)$ , which remains valid for any  $f$  and  $p$  from  $\mathbf{L}_2$ . Let’s multiply the left and the right part of equation (2) by  $A^*$ . Equation (2) can then be re-written as follows:

$$A^*Af = \int \int \frac{f(\xi, \eta) d\xi d\eta}{\sqrt{(x - \xi)^2 + (y - \eta)^2}} = u(x, y), \tag{3}$$

where the function  $u(x, y)$  is defined by the following relation

$$u(x, y) = A^*p = \int_{\theta} p(x \cos(\theta) + y \sin(\theta), \theta) d\theta. \tag{4}$$

In the equation (3), the function  $u(x, y)$  is obtained from the experiment according to the formula (4). The equation (3) depends only on the difference of its arguments. Applying the Fourier transform, we obtain

$$\frac{\tilde{F}(\omega_1, \omega_2)}{\sqrt{\omega_1^2 + \omega_2^2}} = \tilde{U}(\omega_1, \omega_2). \quad (5)$$

Here  $\tilde{F}(\omega_1, \omega_2)$  represents the Fourier image of the function  $f(x, y)$ , and  $\tilde{U}(\omega_1, \omega_2)$  represents the Fourier image of  $u(x, y)$ . Let's rewrite the equation (5) as

$$\tilde{F}(\omega_1, \omega_2) = \sqrt{\omega_1^2 + \omega_2^2} \tilde{U}(\omega_1, \omega_2). \quad (6)$$

The formula (6), in fact, inverts the operator  $A$  and provides an opportunity to write the solution of the original operator equation (2) explicitly in the case where full-range data are provided. Note that if a solution to the problem exists, then, as we have shown, it can be represented as (6), and is therefore the only solution. Applying the inverse Fourier transform to  $\tilde{F}(\omega_1, \omega_2)$  in the representation (6), we can obtain the unknown function  $f(x, y)$ . From the computational perspective, solving the problem (6) is an easy task. The algorithm can be implemented using an ordinary personal computer.

Modern medical CT scanners examine three-dimensional objects. The data collection scheme is designed so that it makes it possible to reconstruct the image in many layers simultaneously. A  $1000 \times 1000 \times 1000$ -point cubical grid is typically used to represent the data for 3D X-ray imaging. The number of two-dimensional sections may reach 1000 for a single patient. Since each of these sections can be reconstructed independently, it is reasonable to use GPUs, which provide at least 100 times speedup when performing the Fourier transform, compared to a single-processor PC. A powerful workstation equipped with several GPU devices is sufficient not only for reconstruction of cross-sections, but also for preliminary image processing, presenting 3D information, etc. [7, 13]. In particular, Digisens Company [6] has developed software for 3D X-ray tomography for GPU clusters.

## 1.2. The problem of reconstructing the image of the Earth's surface from the SAR (Synthetic Aperture Radar) data

The methods of synthesized aperture are used in various fields of wave sensing. One can distinguish two large groups of synthetic aperture radars: aviation-based radars with the resolution up to centimeters, and space-based radars with the resolution of about several meters [14-15]. Such systems are used for monitoring hard-to-reach areas of economic activity (monitoring, classification, assessment of vegetative cover biomass, monitoring of underground pipelines), etc. Synthetic aperture methods are used in medicine as well [16].

The SAR is one of the promising methods of remote examination of the Earth's surface from an aircraft. The use of electromagnetic radiation with the wavelength of about 0.1 m makes it possible to perform the monitoring virtually at any time of day and in all atmospheric conditions.

The main problem in using aircraft-based radars is their low resolving power. Significant remoteness of the radar carrier from the examined area (in case of using spacecraft, the distance may be hundreds of kilometers), natural limits of the size (aperture) of the antenna, sufficiently large wavelength of the probing radiation — all these factors result in an extremely large diameter of the area of interaction of radar radiation with the examined surface, up to several kilometers.

Radar resolution may be improved by using specialized methods of observation based on the principles of synthesized aperture. In remote sensing by synthetic aperture radars, the radar moves along the predetermined path, emits sounding pulses and received reflected signals. By synthesizing a virtual antenna hundreds and thousands of times larger in length than the actual size of the locator, one can improve the resolution by hundreds of times [14, 15, 17].

Processing the data from SAR systems is often performed in real-time. The peculiarity of the SAR image reconstruction problems is the huge volume of input data. It is advisable to use graphics processors [18, 19] to accelerate and parallelize the computations.

The scheme of observations and data recording in a SAR system is shown in fig. 2. A side looking radar is installed on the aircraft and is rigidly connected with the carrier. The radar emits probing signals  $s(t)$  (usually, short pulse signals). The aircraft moves along a rectilinear trajectory above the area being mapped. The reflected signals  $u(t)$  are recorded. The radar equipment allows recording both the amplitude and the phase of reflected signal.

Let's build a mathematical model of the SAR imaging process using the linear approximation. We will use the standard start-stop approximation [14], i.e., we neglect any changes in the geometrical parameters of the "carrier – surface" system during the emission-reception cycle. For the sake of simplicity, we assume that the carrier moves along a straight line parallel to the Earth surface. Such an approximation is acceptable in cases where the carrier trajectory and the terrain may be only slightly curved. However, a priori information about the curvature of the trajectory and the topography of the surface is required for obtaining high-precision images, and in some cases such information is available.

Let's define a Cartesian coordinates system OXYZ on the examined surface (fig. 2). We will assume that the radar carrier moves along a straight line parallel to the OX axis at the height  $H$ . Let us introduce the coordinate  $\xi$  along the carrier's trajectory, so that  $\xi=x$ . For convenience of further presentation, let's translate from the coordinate  $y$  to the coordinate  $\rho$ , where  $\rho = \sqrt{y^2 + H^2}$ . The coordinates  $(x, \rho)$  define a point on the surface and are called the azimuthal distance and the slant-range distance.

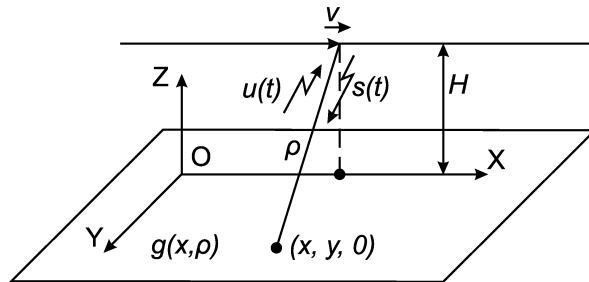


Figure 2. The scheme of synthetic aperture radar

We characterize the reflective properties of the Earth's surface by the coefficient  $g(x, \rho)$ . The function  $g(x, \rho)$  is the sought-for value in the SAR imaging problems. Let's denote the signal emitted by the radar as  $s(t)$ . Due to the principle of superposition, the full signal  $\hat{u}(\xi(t))$  received by the radar at the coordinate  $\xi(t)$  at the moment  $t$ , can be expressed as an integral over the plane of the examined surface  $(x, \rho)$  :

$$\hat{u}(\xi(t)) = \int \int s\left(t - \frac{2R(\xi(t), x, \rho)}{c}\right) P(\xi(t), x, \rho) g(x, \rho) dx d\rho, \quad (7)$$

where  $R(\xi(t), x, \rho)$  is the distance between the radar carrier and the point  $(x, \rho)$  on the surface; the function  $P$  takes into account the beam shape of the antenna; the delay  $\frac{2}{c}R(\xi(t), x, \rho)$  takes into account the duration of signal travel from the carrier to the point  $(x, \rho)$  and back;  $c$  is the speed of radio wave propagation.

Let's specify the probing signals. We will assume that pulse signals are emitted periodically, with the period of  $2T_z$ , in the form of a finite-duration train of high frequency oscillations with the frequency  $\omega_0$ . Let's use the start-stop approximation, assuming that during a period of  $2T_z$  the radar receives reflected signals being at the point  $\xi_j = \xi(t_j) = vt_j$ , which is the coordinate of the carrier along the trajectory, where  $v$  is the speed of the radar carrier movement. In the theory of synthetic aperture,  $t_j$  are called "slow" time. The parameter  $\tau$  is called the "fast" time, and characterizes the slant-range distance from the radar carrier to the point on the studied surface. It can be shown that  $\tau = \text{const}$  corresponds to a segment of the  $y = \text{const}$  line on the ground.

For typical parameters of real radar systems [15], the equation (7) can be approximated as (8), using the second-order approximation [17]. For simplicity, here and further we will omit index  $j$ .

$$u(\xi, \tau) = \int_{\xi-L}^{\xi+L} \exp\left(\frac{i2\omega_0}{c^2\tau}(x-\xi)^2\right) g(x, \tau) dx. \quad (8)$$

In this approximation, the mathematical model of the signal registration in the case of short probing pulses has a form of convolution with the Fresnel kernel in the segment  $(-L, L)$  by the coordinate  $x$  for  $-\infty < \xi < \infty$ . By solving the inverse problem, we obtain the reflectivity coefficient  $g(x, \tau)$  using approximately specified radar data  $u(\xi, \tau)$ .

A characteristic feature of the integral equation (8) is that it breaks down into independent one-dimensional integral equations. For each value of  $\tau$  it is necessary to solve an integral equation of the first kind with the Fresnel kernel, the support set of which is limited to the interval  $(-L, L)$ . For typical radar parameters, the interval  $(-L, L)$  contains hundreds of the Fresnel zones corresponding to the kernel  $\exp(i2\omega_0(x-\xi)^2/(c\rho))$ , which allows obtaining high-resolution image along the  $x$  coordinate using real radar data as input.

For the approximate computation of  $g(x, \tau)$  one can use the following integral operator — "the inverse Fresnel transformation" with finite limits of integration:

$$\tilde{g}(x, \tau) = \int_{-L}^L \exp\left(-\frac{i2\omega_0}{c^2\tau}\xi^2\right) u(x-\xi, \tau) d\xi. \quad (9)$$

In literature, the algorithm (9) is known as the focused synthesis algorithm [15]. As one can see, the focused synthesis algorithm employs a rather simple kind of one-dimensional convolution by the coordinate  $\xi$ . The fast Fourier transform (FFT) procedure can be used to implement the algorithm on a computer.

The data obtained by SAR can cover the size of the Earth's surface up to several tens of kilometers along the azimuthal and slant-range distances. The grid step of the recorded experimental data is about  $1 \times 1$  m. This leads to the need in a huge amount of computations, sometimes performed in real time. However, the specificity of the algorithm is such that the calculations may be performed almost independently for each value of  $\tau$  (the slant-range distance). This makes it possible to efficiently parallelize the calculations by allocating a dedicated range of  $\tau$  values for each parallel process.

Fig. 3 shows the results of digital reconstruction of the image from the SAR mounted on the "Almaz" spacecraft [17]. Fig. 3 shows the original image (on the left) — the  $u(\xi, \tau)$  function obtained by probing the Earth's surface. On the right, fig. 3 shows a fragment of the reconstructed image obtained as a result of solving the inverse problem using the focused synthesis method. As one can see from this example, the use of developed methods allows the resolving power of 11 – 15 m.

Further improvement of the SAR resolving power sets the task of developing mathematical methods and models for SAR image reconstruction. Formulations of the problems in this case are more complicated, because the model includes factors such as curvilinear trajectory of the radar carrier, the effects of the probed terrain surface, the curvature of the operator kernel support set, etc.

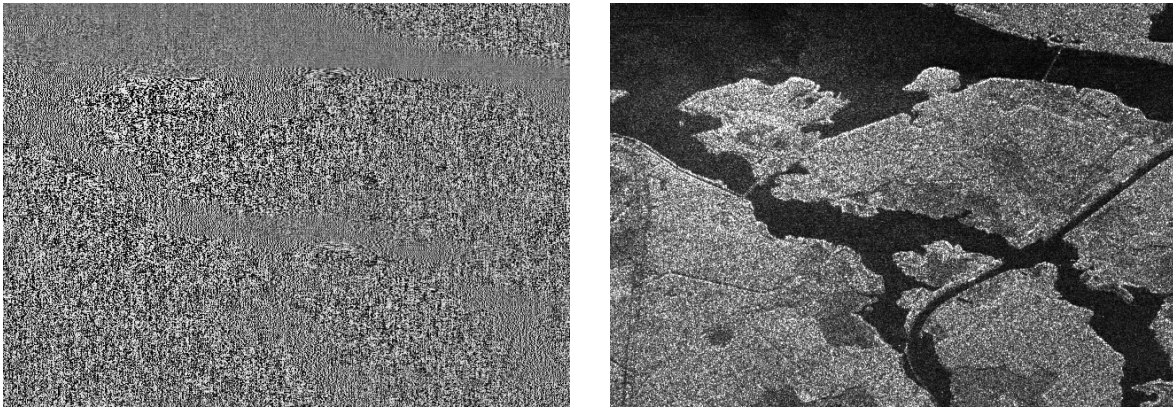


**Figure 3.** Reconstruction of the Earth's surface using the data obtained from the SAR on the "Almaz" spacecraft. Raw data is on the left, reconstructed image is on the right

## 2. The inverse problems of wave tomography in the framework of the integral approach

It has been shown above that efficient algorithms for solving inverse problems of X-ray tomography have been developed, which makes it possible to obtain detailed information about the internal structure of the examined objects. The results in the ultrasonic, acoustic, seismic and electromagnetic tomographic studies are significantly more modest. This is due to the fact that even if we use the simplest scalar wave models, interpreting the results of experiments requires solving complicated nonlinear three-dimensional inverse problems. Due to the significance of wave phenomena, generally speaking, it is incorrect to represent these three-dimensional problems as a set of two-dimensional problems and use the ray-based geometric optics models. Section 2 discusses the integral approach to solving the inverse problem of wave tomography based on the Green function method. Using the integral approach, the inverse problems can be reduced to a system of nonlinear Fredholm integral equations of the first kind [20–22]. The resulting problem is ill-posed. A rich arsenal of iterative methods for solving such problems has been developed [20]. To illustrate solving inverse problems in the integral approach using the iterative methods, we present the model problem of reconstructing the structure of the Earth's near-surface layers using wave sources of radiation. The model problems were solved using the "Lomonosov" supercomputer. The results show that the integral approach is efficient for solving the problems of wave diagnostics on coarse grids only.

### 2.1. Integral formulation of the inverse problem of wave tomography

Propagation of acoustic or electromagnetic radiation in an inhomogeneous medium in the simplest scalar wave approximation is described by the following well-known hyperbolic differential equation:

$$\Delta u(\mathbf{r}, \mathbf{q}, t) - \frac{1}{c^2(\mathbf{r})} u_{tt}(\mathbf{r}, \mathbf{q}, t) = \delta(\mathbf{r} - \mathbf{q})f(t), \tag{10}$$

where  $u(\mathbf{r}, \mathbf{q}, t)$  is a scalar wave field (for example, acoustic pressure in a liquid medium), which depends on the spatial variable  $\mathbf{r} \in \mathbf{R}^3$  and the time  $t \geq 0$ ,  $\Delta$  is the Laplace operator,  $c(\mathbf{r})$  is the velocity of wave propagation,  $\delta(\mathbf{r} - \mathbf{q})f(t)$  describes perturbation of the medium by a point source located at the point  $\mathbf{q} \in \mathbf{R}^3$ ,  $\delta(\cdot)$  is the Dirac's delta function. The initial conditions at  $t=0$  are  $u(\mathbf{r}, \mathbf{q}, 0)=0$ ;  $u_t(\mathbf{r}, \mathbf{q}, 0)=0$ .

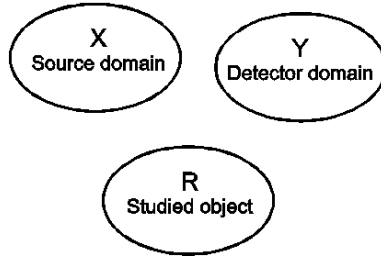


Figure 4. Scheme of tomographic examinations

Let us consider the following well-known general formulation of the inverse problem (fig. 4). Let the inhomogeneity of the medium be localized in the domain R. Let us assume that the sounding wave sources (positions of which are characterized by the vector  $\mathbf{q}$ ) are located in the domain X ( $\mathbf{q} \in X$ ), and the detectors that measure the wave field  $u(\mathbf{r}, \mathbf{q}, t)$  are present only in the domain Y ( $\mathbf{r} \in Y$ ). The domain R does not intersect with the domains X and Y, while X and Y may overlap or coincide. We will assume that  $c(\mathbf{r})$  is a smooth function, which differs from the known constant  $c_0$  only within the domain R ( $0 < c_1 < c(\mathbf{r}) < c_2$ ). The function  $f(t)$  that describes the initial pulse is known a priori. In the inverse problem, we are to determine the unknown function  $c(\mathbf{r})$ ,  $\mathbf{r} \in R$ , using experimental data  $u(\mathbf{r}, \mathbf{q}, t)$  obtained for  $\mathbf{r} \in Y$ . Such an inverse problem is nonlinear, since the function  $u(\mathbf{r}, \mathbf{q}, t)$  is unknown, where  $\mathbf{r} \notin Y$ .

Above, the problem has been formulated in the time domain. Let us present the formulation in the frequency domain. Applying the Fourier transform by the time variable  $t$  to the left and right part of the equation (10), the problem may be reduced to the Helmholtz equation, when the source is a point harmonic oscillator

$$\Delta u(\mathbf{r}, \mathbf{q}, \omega) + k^2(\mathbf{r}, \omega) u(\mathbf{r}, \mathbf{q}, \omega) = f(\mathbf{r}, \mathbf{q}, \omega), \tag{11}$$

where  $k(\mathbf{r}, \omega) = \omega/c(\mathbf{r})$ . In the scalar approximation, this equation describes the acoustic or electromagnetic field  $u(\mathbf{r}, \mathbf{q}, \omega)$  generated by the source described by the function  $f(\mathbf{r}, \mathbf{q}, \omega)$ . If the source is located at the point  $\mathbf{q} \in X$ , this function assumes the form  $f(\mathbf{r}, \mathbf{q}, \omega) = -\delta(\mathbf{r}-\mathbf{q})$ , where  $\omega$  is the circular frequency of the sounding wave source. Inhomogeneity of the medium is caused only by changes in the phase velocity  $c(\mathbf{r})$ . Outside the inhomogeneous region  $k(\mathbf{r}, \omega) = k_0 = \omega/c_0$ , where  $c_0=const$  is known.

In this inverse problem, same as above, we are to determine the unknown function  $c(\mathbf{r})$ ,  $\mathbf{r} \in \mathbb{R}$ , using experimental data  $u(\mathbf{r}, \mathbf{q}, \omega)$  obtained at points  $\mathbf{r} \in Y$  for some set of frequencies  $\omega$  and source positions  $\mathbf{q} \in X$ .

Let's consider the well-known approach to solving coefficient inverse problems in the framework of frequency-domain wave models, which is based on integral representation using the Green function. It is well known that the Green function for the equation (11) in a homogeneous medium satisfies the equation

$$\Delta G(\mathbf{r}, \mathbf{q}, \omega) + \frac{\omega^2}{c_0^2} G(\mathbf{r}, \mathbf{q}, \omega) = -\delta(\mathbf{r} - \mathbf{q})$$

and has the form

$$G(\mathbf{r}, \mathbf{q}, \omega) = \frac{1}{4\pi \|\mathbf{r} - \mathbf{q}\|} \exp(i \frac{\omega}{c_0} \|\mathbf{r} - \mathbf{q}\|).$$

Same as before, we assume that the wave field  $u(\mathbf{r}, \mathbf{q}, \omega)$  is measured in the domain  $Y$  ( $\mathbf{r} \in Y$ ), i.e., the detectors run through the domain  $Y$ . The point sources run through the domain  $X$  ( $\mathbf{q} \in X$ ), the studied inhomogeneity is located in the compact domain  $\mathbb{R}$ . By writing the equations separately for the domains  $\mathbb{R}$  and  $Y$ , we will obtain the following nonlinear system of equations

$$F(Z) = 0, \tag{12}$$

where

$$F(Z) = \begin{cases} u(\mathbf{r}, \mathbf{q}, \omega) - u_0(\mathbf{r}, \mathbf{q}, \omega) - \omega^2 \int_{\mathbb{R}} G(\mathbf{r}', \mathbf{r}, \omega) \xi(\mathbf{r}') u(\mathbf{r}', \mathbf{q}, \omega) d\mathbf{r}', & \mathbf{r} \in \mathbb{R} \\ \omega^2 \int_{\mathbb{R}} G(\mathbf{r}', \mathbf{p}, \omega) \xi(\mathbf{r}') u(\mathbf{r}', \mathbf{q}, \omega) d\mathbf{r}' - U(\mathbf{p}, \mathbf{q}, \omega), & \mathbf{p} \in Y \end{cases}.$$

Here  $U(\mathbf{p}, \mathbf{q}, \omega) = u(\mathbf{p}, \mathbf{q}, \omega) - u_0(\mathbf{p}, \mathbf{q}, \omega)$ ,  $u_0(\mathbf{r}, \mathbf{q}, \omega) = -\int_X G(\mathbf{r}', \mathbf{r}, \omega) f(\mathbf{r}', \mathbf{q}, \omega) d\mathbf{r}'$ ,  $\xi(\mathbf{r}) = c_0^{-2} - c^{-2}(\mathbf{r})$ ,  $Z = (\xi(\mathbf{r}), u(\mathbf{r}, \mathbf{q}, \omega))$ .

The equation (12) is an integral equation of the first kind in certain Hilbert spaces with respect to  $\xi(\mathbf{r})$  and  $u(\mathbf{r}, \mathbf{q}, \omega)$ . This equation is nonlinear, since the equation contains unknown functions as a product.

In this inverse problem, the properties of the medium  $\xi(\mathbf{r})$  and the wave field  $u(\mathbf{r}, \mathbf{q}, \omega)$  are considered unknown. The function  $U(\mathbf{p}, \mathbf{q}, \omega)$  is obtained by measurement and is known in the domain  $\mathbf{p} \in Y$ ,  $\mathbf{q} \in X$  for some set of frequencies  $\omega$ . The problem is to reconstruct the inhomogeneity of the medium  $\xi(\mathbf{r})$  using these measurements.

## 2.2. Iterative algorithms for solving inverse problems of wave tomography in the integral approach

The resulting problem (12) is ill-posed and can be solved, for example, using the iterative-regularized Gauss — Newton method described in [20]

$$Z_{s+1} = Z_s - (F'_s{}^* F'_s + \alpha_s E)^{-1} (F'_s{}^* F(Z_s) + \alpha_s (Z_s - \zeta)), \tag{13}$$

where  $s$  is the iteration number,  $F'_s = F'(Z_s)$  is the Frechet derivative for (12),  $F'_s{}^*$  is the adjoint operator to  $F'_s$ . The suitable choice of the sequence  $\alpha_s$  and the element  $\zeta$  ensures regularizing properties of the algorithm.

It turns out that one can explicitly write down the formulas for  $F'_s = F'(Z_s)$  and  $F'^*_s F'_s$  [23]. However, even an ability to write explicit expressions for the matrices does not make it possible to effectively solve the inverse problem in question. The fact is that this task is extremely computationally expensive. The number of unknown values in the problem grows approximately as  $O(tn^3)$ , where  $n$  is the number of points in one direction of a three-dimensional grid,  $t = N_\omega \cdot N_q$ , where  $N_\omega$  is the number of probing frequencies,  $N_q$  is the number of source positions.

In this Gauss – Newton procedure (13), the most computationally expensive operations are computing the matrix  $F'^*_s F'_s$  and inverting the operator  $(F'^*_s F'_s + \alpha_s E)$  at the each iteration of the Gauss–Newton procedure. It takes about  $O(tn^9)$  addition and multiplication operations to compute the matrix. To invert the operator using an iterative methods it takes about  $O(tn^6)$  operations at each step, and the number of steps is typically several hundred [24].

Such tasks with  $n > 20$  cannot be solved on a personal computer. A simple assessment shows that even if the computational power of the system is increased by 1000 times, we would only be able to increase the grid size by 2 times. Therefore, the presented integral algorithms are effective only on coarse grids.

### 2.3. Model calculations of inverse problems of wave tomography in integral formulation

To assess efficiency of the algorithms proposed in section 2.2, the model problems of reconstructing the structure of the Earth’s subsurface layer have been solved [22, 23]. Numerical experiments have been performed with the use of the ”Chebyshev” supercomputer. Iterative regularized Gauss–Newton method (13) was used to solve 3D inverse problems of wave tomography; the matrix was inverted using iterative methods that consisted of repeated vector-matrix multiplication operations. The advantage of such iterative methods, compared to direct methods of matrix inversion, is the possibility of parallelization — each parallel process has to store only several rows of the matrix and multiplies only these rows by the vector. Bearing in mind that the number of rows in the matrix can be up to several tens of thousands, such parallelization is very effective and, importantly, scalable to many processes.

In the problems of seismic surveys, sources and detectors are generally located on the Earth’s surface. This, of course, imposes limitations on the resolving power of seismic methods. The situation in civil engineering, where small areas with dimensions of tens of meters are studied, is somewhat better. In this case, one can position the sources and detectors not only on the surface, but in the boreholes, surrounding the area being examined. Fig. 5 shows a layout of a model experiment (sources are marked with cones, detectors are marked with points). Sources and detectors were located on the Earth’s surface (in the  $z=0$  plane) in a  $20 \times 20$  m area, and in vertical boreholes up to 10 m deep. The inhomogeneity (numerical phantom) was chosen in the form of two cubes. The dimensions of the cubes were 3 m and 6 m, the grid size was 1.5 m. The phase velocity was equal to  $2000 \text{ m}\cdot\text{s}^{-1}$  in the cubes and  $1000 \text{ m}\cdot\text{s}^{-1}$  in the surrounding volume. The problem was solved at the single frequency  $\omega = 100 \text{ Hz}$ . Fig. 6 shows a cross section of the reconstructed image in the plane OYZ on a  $18 \times 18 \times 18$ -point grid.

As one can see from the numerical experiments, the nonlinear inverse problem in the integral representation is too computationally expensive to solve even on modern supercomputers. Even if 512 processor cores are used, computations can be performed in a reasonable time only on a  $20^3$ – $30^3$ -point grid, which is insufficient for complex tasks involving real measured data. As

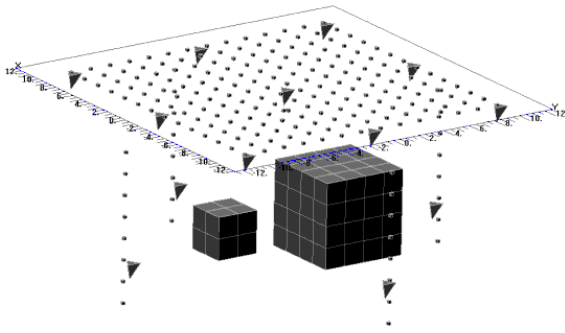


**Figure 5.** Layout of the numerical experiment with boreholes

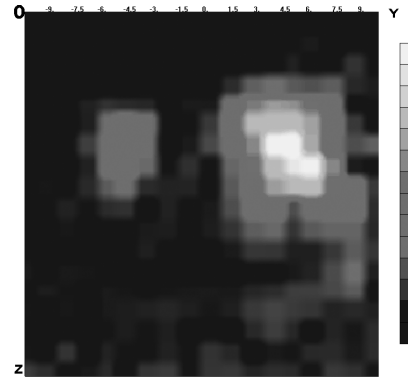


**Figure 6.** Cross-section in the OYZ plane of the reconstructed 3D image on a  $18 \times 18 \times 18$ -point grid

the number of grid points increases, the number of operations required to solve the 3D inverse problem using the integral approach increases as  $n^9$ , where  $n$  is the number of grid points along either one coordinate. Thus, for obtaining more detailed information that is characteristic for tomography, it does not seem possible to implement the integral approach.

The natural solution in this case is linearization of integral equations (Born, Rytov approximations, etc.) [20]. Using of linearized approximations in the integral approach reduces significantly the amount of computations. However, the possibility of application of these approximations to real problems for complex heterogeneous media is rather limited due to the fact that the model is simplified. However, linearized approximations may be used in the case of a simple structure of the studied object (e.g., localized small inhomogeneities) or for obtaining the initial approximations for iterative procedures to solve nonlinear inverse problems.

### 3. Differential approach to inverse problems of wave tomography

In the previous section, the integral approach has been discussed. From the formal point of view, there are algorithms that are quite suitable for solving the obtained system of integral equations. However, implementation of these algorithms even on modern supercomputers is very difficult. Therefore, simplified models seem to be attractive in application to solving 3D problems of wave tomography.

The simplest model is the linear ray-based model similar to X-ray tomography, in which the ultrasonic pulses' travel time between sources and detectors is measured. Such models have been first used in the 70-ies [25] and are called time-of-flight (TOF) tomography. The integrals of the sound speed along the rays are obtained by measurements, and the sound speed distribution inside the object may be reconstructed using the inverse Radon transform (2). However, unlike X-rays, which practically do not deviate from straight lines, ultrasonic waves are subject to refraction, diffraction, multiple scattering, etc. Therefore, the ray model does not work well in heterogeneous media, and the reconstructed images are of poor quality. The advantage of the linear model is its simplicity and a possibility to implement the method even on a personal computer.

The ray model may be improved by introducing a correction for refraction. Having obtained a rough approximation of the sound speed using the linear model, one can plot the trajectories of

the rays through the object with regard to refraction and measure the time of pulse arrival along the new ray path, thus defining the velocity structure with higher accuracy. This problem is a nonlinear one, and iterative methods are used to solve it. The required amount of computations is significantly greater than for the linear model, and graphics accelerators are used for image reconstruction [26].

Knowing the approximate velocity distribution, one can use the reflected ultrasonic waves for obtaining the reflectivity image. This method is called refraction-corrected reflection [8]. Without knowing the sound velocity, it is impossible to link the reflection to a specific point of the object. This leads to distortion of the reflectivity image obtained with regular, non-tomographic devices. The refraction-corrected reflection method allows obtaining a more accurate image; however, it has several disadvantages. First of all, the reflectivity image carries no information about parameters of the tissue, but only about the shape of the inhomogeneity's boundaries. Secondly, the ray model does not take into account diffraction effects, which become significant when the size of inhomogeneities is about 1–2 wavelengths. As a result, speed of sound image, which could be used for tissue characterization, though is better than in the linear model, still has too low quality for a number of tasks, such as early cancer diagnosis.

In the three dimensional variant, one can attempt to use the synthetic aperture method for tomographic image reconstruction. Presenting an unknown object as a set of points that scatter ultrasonic radiation in all directions, it is possible to determine accurately the coordinates of these points. However, the model of the synthesized aperture works well only in a homogeneous media. Diffraction can be partially taken into account, but accounting for refraction and multiple scattering in such a model is difficult. The resulting reflectivity image still has no information about the type of the tissue, but only about the shape of inhomogeneities. Implementation of the 3D method requires fairly large amount of computation, and GPU clusters are to be used [16].

Wave models describe ultrasound wave propagation in the tissue most accurately, and therefore make it possible to use the results of the measurements to the most extent. However, the inverse problems of image reconstruction for wave models are nonlinear and very complicated. The described above integral approach requires  $n^9$  operations for solving a 3D problem on a  $n^3$  grid. In a simplified formulation of parabolic approximation, the wave methods are developed in the work [8].

In recent years, breakthrough results have been achieved in the field of inverse problems of wave tomography [27–29]. In these works, the inverse problem of wave tomography is formulated as a coefficient inverse problem for a wave equation. The developed gradient-descent methods for solving inverse problems using the differential (FDTD) approach make it possible to solve the 3D problem of tomographic image reconstruction using just  $n^4$  operations. With the help of the gradient methods, one can obtain a sound speed image, the accuracy of which is limited only by the accuracy of the measurements performed, and by the adequacy of the mathematical model to the real wave propagation processes. In practice, the computations may be performed in reasonable time using powerful graphics clusters containing about 30–40 GPU devices. Such clusters may be used as computing devices in medical and other tomographic systems. With the constant improvement of the technology, performance of the devices increases and power consumption decreases; this will make possible the mass use of such computing devices in ultrasonic tomographic systems for diagnosing breast cancer.

### 3.1. Formulation of the inverse problem of wave tomography as a coefficient inverse problem for wave equation

Let us consider the problem of reconstructing an unknown sound speed inside an object using the data obtained by a tomographic examination. First, let us consider a two-dimensional problem. Despite the fact that the process of wave propagation in an inhomogeneous medium is always three-dimensional, 2D (layer-by-layer) measurements make it possible to obtain acceptable image quality in some applications. Implementation of a layer-by-layer model requires much simpler equipment and less amount of computation.

The scheme of 2D (layer-by-layer) tomography is shown in fig. 7. The studied object  $G$  is placed in the homogeneous medium  $L$  with known properties. At the border of the examined area there are ultrasound sources 1 and detectors 2.

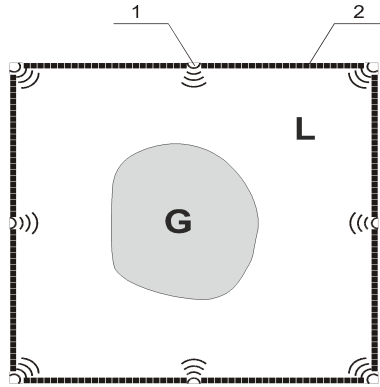


Figure 7. Scheme of 2D tomography

We will use a simple scalar wave model that describes pressure waves in liquid media. It is applicable for soft tissues, too. The acoustic pressure  $u(\mathbf{r}, t)$  satisfies the equation

$$c(\mathbf{r})u_{tt}(\mathbf{r}, t) - \Delta u(\mathbf{r}, t) = \delta(\mathbf{r} - \mathbf{q}) f(t) \tag{14}$$

$$u(\mathbf{r}, t = 0) = u_t(\mathbf{r}, t = 0) = 0, \quad \partial_n u|_{ST} = p(\mathbf{r}, t). \tag{15}$$

Here  $c^{-0.5}(\mathbf{r}) = v(\mathbf{r})$  is the speed of ultrasound propagation,  $\partial_n u|_{ST}$  is the derivative along the normal to the surface  $S$  in the domain  $S \times (0, T)$ ,  $\delta(\mathbf{r} - \mathbf{q})f(t)$  describes the initial pulse emitted by a point source at the point  $\mathbf{q} \in \mathbf{R}^2$ ,  $\Delta$  is the Laplace operator. Let us assume that heterogeneity of the studied object is caused only by the changes in the sound speed  $c(\mathbf{r})$ , while the sound speed in the medium  $L$  is constant and known,  $c(\mathbf{r})=c_0=\text{const}$ . The function  $p(\mathbf{r}, t)$  is also known. The inverse problem consists in finding unknown sound speed  $c(\mathbf{r})$ , which is a coefficient in the differential equation (14), using the measured acoustic pressure  $U(\mathbf{s}, t)$  at the detectors  $\mathbf{s} \in S$  during the time  $(0, T)$  with different positions of the ultrasound source  $\mathbf{r}_0$ . The inverse problem is formulated as a problem of minimization of the quadratic residual functional  $\Phi(u(c))$  by  $c$ .

$$\Phi(u(c)) = \frac{1}{2} \int_0^T \int_S (u(\mathbf{s}, t) - U(\mathbf{s}, t))^2 \, d\mathbf{s} \, dt.$$

### 3.2. Representation of the gradient of the residual functional

We use gradient iterative methods to minimize the residual functional. Breakthrough results in solving coefficient inverse problems are associated with the possibility to formulate explicitly and compute the gradient  $\Phi'(u(c))$  of the residual functional. In various formulations, the expression for the gradient has been derived in the works [27, 28, 24, 30]. According to [24], the gradient of the residual functional for the inverse problem (14–15) has the following form:

$$\Phi'_c(u(c)) = \int_0^T w_t(\mathbf{r}, t) u_t(\mathbf{r}, t) dt. \quad (16)$$

Here  $u(\mathbf{r}, t)$  is the solution of the primary problem (14–15), and  $w(\mathbf{r}, t)$  is the solution of the "conjugate" problem:

$$c(\mathbf{r}) w_{tt}(\mathbf{r}, t) - \Delta w(\mathbf{r}, t) = 0, \quad (17)$$

$$w(\mathbf{r}, t = T) = w_t(\mathbf{r}, t = T) = 0, \quad \partial_n w|_{ST} = u|_{ST} - U. \quad (18)$$

Thus, for computing the gradient of the residual functional, it is necessary to solve both the main and the "conjugate" problems. Knowing  $\Phi'_c$  from (16), we can build various iterative schemes for gradient minimization of the residual functional.

### 3.3. Numerical methods for solving coefficient inverse problems of wave tomography

We will use the finite-difference time-domain method (FDTD) to solve the inverse problem. In this formulation, solving the differential wave equations is reduced to solving algebraic finite-difference equations. For the sake of simplicity, we describe the two-dimensional version of the method. We define a uniform discrete grid in the computational domain:

$$v_{ijk} = \{(x_i, y_j, t_k) : x_i = ih, 0 \leq i < n; y_j = jh, 0 \leq j < n; t_k = k\tau, 0 \leq k < m\},$$

where  $h$  is the grid step for spatial variables,  $\tau$  is the time step. Let's use the following second-order approximation for second derivatives in the equation (14):

$$u_{tt}(\mathbf{r}, t) = \frac{u_{ij}^{k+1} - 2u_{ij}^k + u_{ij}^{k-1}}{\tau^2}, \quad u_{xx}(\mathbf{r}, t) = \frac{u_{i+1j}^k - 2u_{ij}^k + u_{i-1j}^k}{h^2}.$$

A similar finite-difference scheme is used for  $u_{yy}(\mathbf{r}, t)$ . In the area excluding the ultrasound sources, we obtain an explicit scheme for differential equation (14) for calculating the wave field  $u$  at the next time step ( $k+1$ ):

$$u_{ij}^{k+1} = \frac{1}{c_{ij}} \tau^2 \Delta u_{ij}^k + 2u_{ij}^k - u_{ij}^{k-1}, \quad (19)$$

where  $\Delta u_{ij}^k = \frac{1}{h^2} \left\{ (u_{i+1j}^k - 2u_{ij}^k + u_{i-1j}^k) + (u_{ij+1}^k - 2u_{ij}^k + u_{ij-1}^k) \right\}$  is a two-dimensional discrete Laplacian at the point  $(i, j)$  at the time step  $k$ ;  $u_{ij}^k$  is the value of  $u(\mathbf{r}, t)$  at the same point,  $c_{ij}$  is the value of  $c(\mathbf{r})$  at the point  $(i, j)$ . Parameters  $h$  and  $\tau$  are connected by the Courant–Friedrichs–Lewy stability condition:  $c^{-0.5}\tau < \frac{h}{\sqrt{2}}$ . The time  $T$  is chosen long enough so that

all ultrasonic waves have time to reach the detectors, and the signal level  $U(\mathbf{s}, t)$  for  $t > T$  is negligible.

The gradient  $\Phi'_c$  (4) is computed using the following formula

$$(\text{grad } \Phi)_{ij} = \sum_{k=0}^m \frac{u_{ij}^{k+1} - u_{ij}^{k-1}}{2\tau} \frac{w_{ij}^{k+1} - w_{ij}^{k-1}}{2\tau} \tau. \quad (20)$$

For the three-dimensional variant, the FDTD formulas are similar. Three-dimensional Laplacian can be approximated as described in [31].

We used the following iterative process to minimize the residual functional (4). For the initial approximation, we assume  $c^{(0)} = c_0 = \text{const}$ . At each iteration ( $m$ ), the following steps are performed:

1. Calculation of the initial pulse from each source.
2. Solving the direct problem (14–15) for the current iterative approximation  $c^{(m)}$ . Propagation of the ultrasonic wave field  $u^{(m)}(\mathbf{r}, t)$  is calculated by formula (19). Values of  $u(\mathbf{s}, t)$  are calculated at the detectors  $\mathbf{s}$ .
3. Calculation of the residual functional  $\Phi^{(m)} = \Phi(u^{(m)}(\mathbf{r}))$ .
4. Solving the “conjugate” problem (17–18) for  $w^{(m)}(\mathbf{r}, t)$ .
5. Calculation of the gradient by formula (20) for all the sources. The gradient  $\text{grad}\Phi^{(m)}$  is the sum of gradients obtained for each source.
6. Correction of the current iterative approximation:  $c^{(m+1)} = c^{(m)} + \lambda^{(m)} \text{grad } \Phi^{(m)}$ . The process returns to stage 2.

The increment  $\lambda^{(m)}$  is determined from a priori considerations. During subsequent iterations,  $\lambda^{(m)}$  is increased if  $\Phi^{(m)} < \Phi^{(m-1)}$  and decreased if  $\Phi^{(m)} \geq \Phi^{(m-1)}$ . It takes 50 – 200 gradient descent iterations to find the solution, depending on the tomographic scheme and accuracy of measurements.

### 3.4. Numerical simulations of layer-by-layer ultrasonic tomography problems

The tomographic scheme and the parameter values for the numerical experiments were chosen primarily for the purpose of modeling the problem of breast ultrasound tomography. We used the mathematical model described by the equation (14–15). Modeling was performed according to the scheme in fig. 7. First, we computed acoustic pressure  $U(\mathbf{s}, t)$  at the detectors for the given sound speed distribution  $c(\mathbf{r})$ , and then we solved the inverse problem: the sound speed  $c(\mathbf{r})$  was reconstructed using the data  $U(\mathbf{s}, t)$  at the detectors.

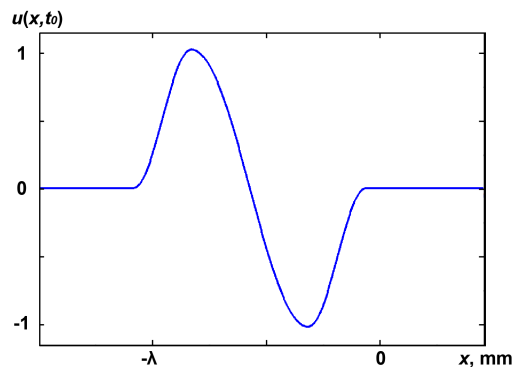
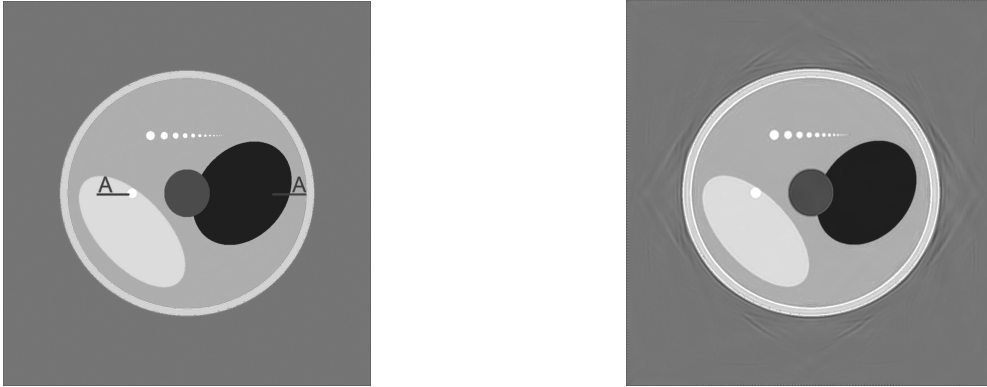


Figure 8. Waveform of the initial pulse

Waveform of the initial pulse is shown in fig. 8. For a 2D model, the following values of parameters were used: pulse width  $\lambda=5$  mm, sound speed range within the object — 1.43–1.6  $\text{km} \cdot \text{s}^{-1}$ , in the medium — 1.5  $\text{km} \cdot \text{s}^{-1}$ , the size of the computational domain  $h=204$  mm, FDTD grid size  $1024 \times 1024$  pixels. Eight sources were used in the numerical experiment, by two on each side of the square. The detectors were located around the perimeter of the square at the distance of 0.8 mm from each other.



**Figure 9.** The two-dimensional numerical experiment: exact image (numerical phantom) – (left); reconstructed image – (right)

Fig. 9 (left) shows the numerical sound speed phantom, fig. 8 (right) shows the reconstructed image. As one can see in the figures, in such a configuration of sources and detectors, the image may be reconstructed quite accurately even when using a small number of sources, assuming that measurement errors are sufficiently low. The computing time for solving a 2D problem using 8 NVIDIA Tesla X2070 graphics processors (one for each source) was about 30 minutes, with 200 iterations performed.

### 3.5. Applicability of the layer-by-layer models to solving three-dimensional problems of wave tomography

The use of layer-by-layer tomographic schemes is not strictly justified for ultrasonic applications. This idea has been borrowed from X-ray tomography, where the use of layer-by-layer examination is possible due to the fact that X-rays almost do not deviate from a straight line. In ultrasonic tomography, the hope for allocating thin layers similar to X-ray tomography is not always justified, because the rays can bend due to refraction both within the studied two-dimensional layer and in the third dimension, and leave the layer. Such wave phenomena as diffraction and multiple scattering aren't taken into account by the ray-based model too.

We performed numerical simulations to study the possibility of using two-dimensional layer-by-layer schemes for ultrasonic tomographic reconstruction of 3D objects. Such studies are of interest because of great popularity of the layered approach in ultrasonic tomography [1, 29, 32, 33]. In this paper we focus on the task of differential diagnostics of breast cancer, which requires resolving small-sized and low-contrast inhomogeneities in the medium.

The scheme of the numerical experiment is shown in fig. 10. It shows a cubic computational domain, inside which the simulation of ultrasonic wave interaction with the object  $\Omega$  (designated as 1) was performed. We chose the simplest three-dimensional object — a homogeneous ball placed in a homogeneous medium. The choice of a ball as a test object was determined by the fact that for a spherically symmetric object it is possible to obtain explicitly the analytical solution

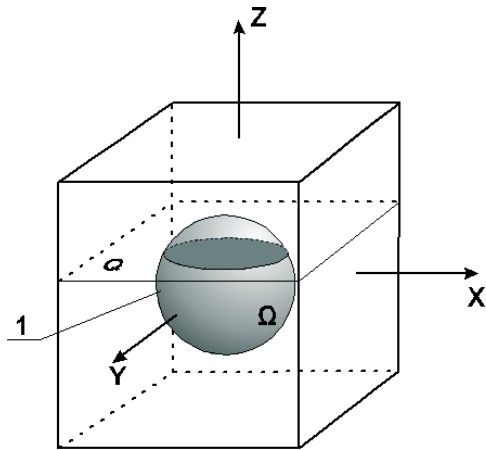


Figure 10. Scheme of the 3D numerical experiment

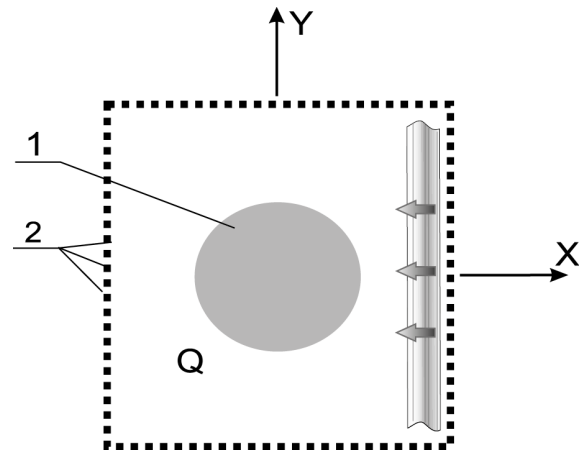


Figure 11. Scheme of the 2D numerical experiment

for the direct problem of pressure-wave propagation using decomposition by special functions (Legendre polynomials and spherical Hankel functions of the second kind). This approach has been well studied in literature [34]. Using the method of decomposing the solution into series of special functions, it is possible to calculate the wave field at any point in the selected plane  $Q$  of three-dimensional space that crosses the ball. This way, we solve the three-dimensional forward problem of wave propagation. Next, we solve the two-dimensional inverse problem (fig. 11) based on the data at the detectors (designated as 2) in the plane  $Q$  using numerical methods, and then we can compare the obtained result with the exact cross-section of the ball (designated by the digit 1).

The center of the cube is located at the point of reference, the  $Z$  axis is directed upwards. The size of the cube is  $20 \times 20 \times 20$  cm. The homogeneous medium has the density of  $1 \text{ g/cm}^3$  and the sound speed of  $c_0 = 1500 \text{ m}\cdot\text{s}^{-1}$  (water). The inhomogeneity has a spherical shape with radius of 6 cm and the sound speed of  $c_\Omega = 1600 \text{ m}\cdot\text{s}^{-1}$ . The density of the ball is assumed to be equal to the density of the environment,  $1 \text{ g/cm}^3$ .

A plane wave falling on the ball from four sides along the  $X$  and  $Y$  axes (indicated by arrows on fig. 11) was used as the sounding wave for analytical solution of the direct problem in 3D. The pulse width was  $\lambda = 7$  mm. The distance between the detectors located on the sides of the examined cross-section  $Q$  did not exceed  $\lambda/3$ .

For the purpose of studying the possibilities of using layer-by-layer schemes for 3D wave-tomography imaging, two-dimensional inverse problems were solved numerically in various cross-sections  $Q$  perpendicular to the  $Z$ -axis. For numerical solution of 2D inverse problems, the size of cross-section  $Q$  was  $20 \times 20$  cm, FDTD grid size was  $1000 \times 1000$  pixels.

Fig. 12 b shows the reconstructed velocity structure in the planes  $z = 0$  cm, and  $z = 4$  cm, where the plane  $z=0$  passes through the center of the ball. Fig. 12 a shows the exact cross-sections of the ball for the same  $z$ . It can be seen that for the central cross-section  $z = 0$ , the reconstructed solution coincides with the exact solution quite well. With increasing  $z$ , the effect of refraction increases too, this results in distortion of the shape and appearance of artifacts.

Thus, we can assume that in principle the layer-by-layer scheme is applicable to ultrasound tomography, it is possible to obtain both the shape of the heterogeneous object (albeit with some inaccuracy) and the absolute sound speed value. However, the use of layer-by-layer schemes can lead to the distortion of geometrical shape, appearance of artifacts; the images are blurred along

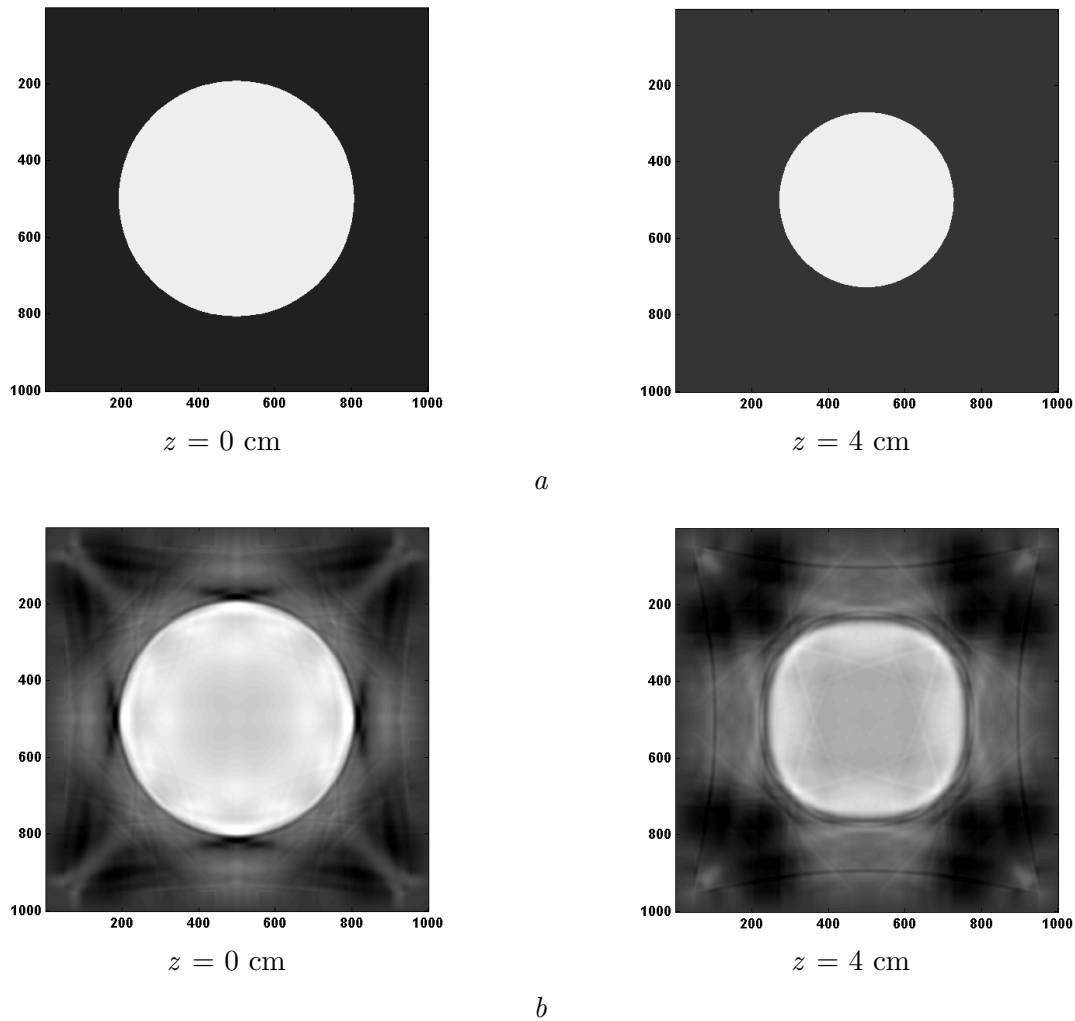


**Figure 12.** The model problem of reconstruction of a three-dimensional ball: *a* — ball cross-sections in planes  $z=\text{const}$ , *b* — reconstructed images

the Z-axis, which is consistent with the results of [35]. The problems that occur in layer-by-layer tomography can be most easily described at the physical level as restrictions of the ray-based approximation. Unlike X-rays, ultrasonic beams are not straight lines. Moreover, they can leave the studied cross-section. These issues restrict the use of layer-by-layer imaging schemes.

### 3.6. Numerical simulations. The three-dimensional formulation of the inverse problem

In the three-dimensional numerical simulation of wave-tomography imaging, the studied object was placed inside a cubic computational domain, at the borders of which the sources and detectors were located. The scheme of the numerical experiment is shown in fig. 13. The ultrasound sources  $S$  were placed at 24 positions in two planes  $z=h_0$  and  $z=h_1$ . The pulse width (wavelength)  $\lambda$  was chosen as 5 mm, the sound speed range inside the object was  $1.43 - 1.6 \text{ km}\cdot\text{s}^{-1}$ , the sound speed in the medium was  $1.5 \text{ km}\cdot\text{s}^{-1}$ .

The detectors were located on the faces of the  $176 \times 176 \times 176 \text{ mm}$  cubic computational domain  $\Omega$ , including the bottom face  $z=0$  and top face  $z=H$ . The distance between the adjacent detectors was 2 mm. Thus, each face of the cube is an array of  $54 \times 54$  detectors. The cross-sections of the reconstructed 3D sound speed image in the  $z=\text{const}$  planes are shown in fig. 14,

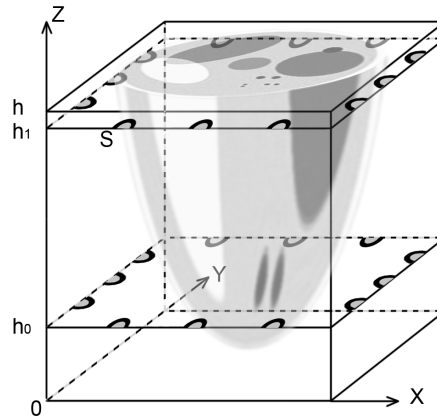


**Figure 13.** Scheme of the 3D numerical simulation

and in the  $y=const$  planes in fig. 15. It can be seen that in this scheme even the smallest inclusions (diameter of which in this example is about 1 mm) are well reconstructed.

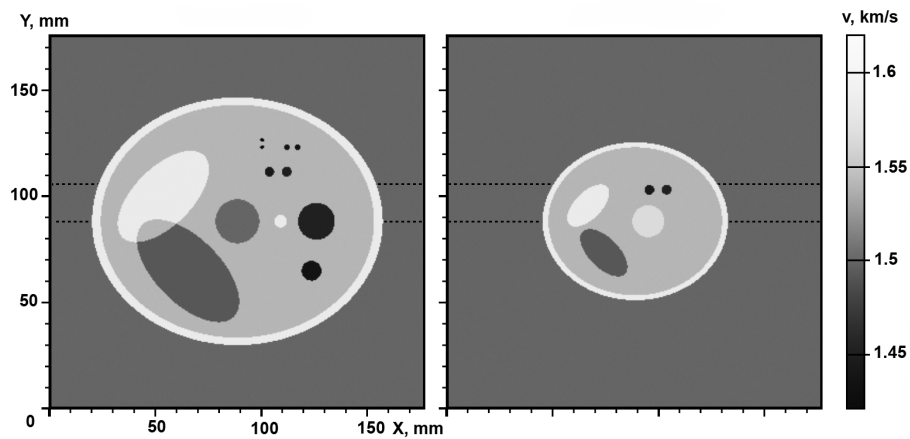


**Figure 14.** Cross-sections of the reconstructed 3D image in  $z = const$  planes

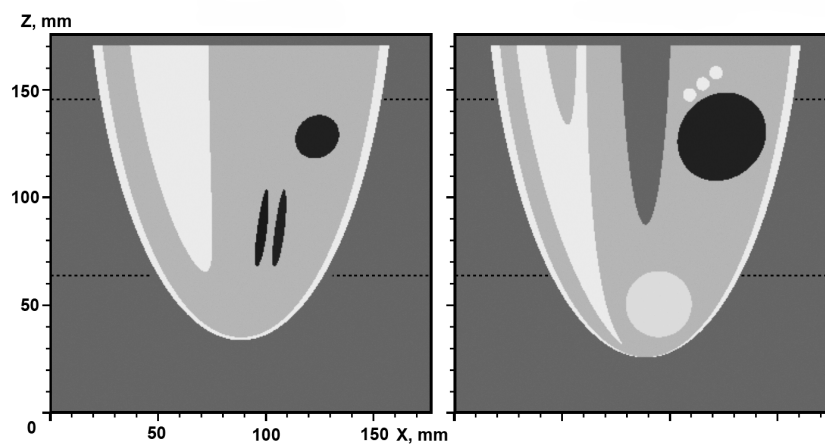


**Figure 15.** Cross-sections of the reconstructed 3D image in  $y = const$  planes

The 3D problems were solved on a  $352 \times 352 \times 352$  - point FDTD grid. The time of computing a 3D task on a cluster of 24 NVidia Tesla X2070 devices was about 2 hours, 150 gradient descent

iterations have been performed. As one can see from the figures, the sound speed image is reconstructed fairly well. Note that solving an inverse problem with over 30 million unknowns required less than 20 thousand detectors. Reconstructing a similar 3D image using a ray model would have required several million rays. Modern X-ray tomographs use up to  $10^9$  rays. It is almost impossible to implement such a number of ultrasonic detectors. One of the advantages of the wave model is the possibility of reconstructing the tomographic image using a much smaller number of sources and detectors, since the wave model uses all of the information about the wave field  $u(\mathbf{r}, t)$  obtained from the detectors. Using large amounts of information indicates the increase of complexity of image reconstruction algorithms, and the necessity of using supercomputers.

### 3.7. The problems of designing ultrasonic tomography devices for medical examinations

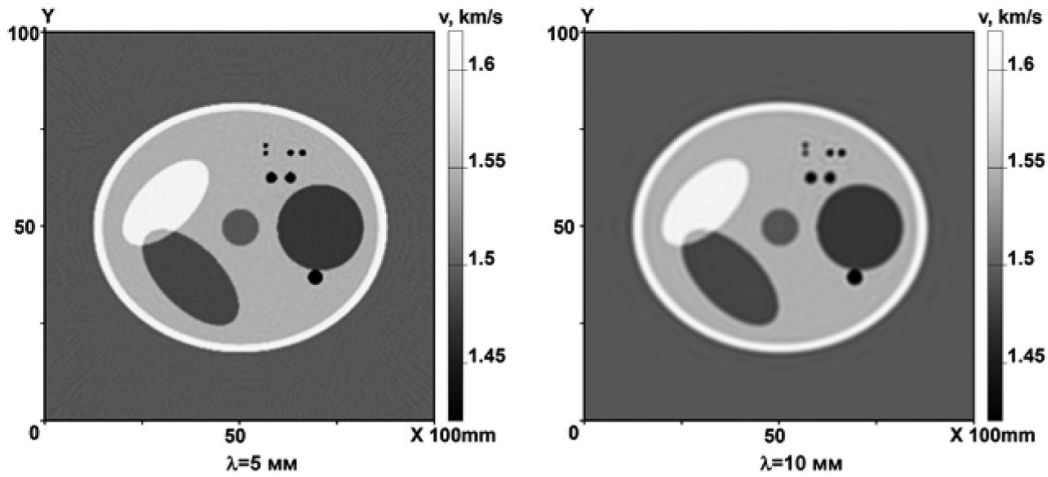
The developed algorithms and software make it possible to perform numerical simulations for various parameters of the experiment, such as the waveform of the sounding pulse, the number and location of sources and detectors, accuracy of measurement, etc. Supercomputer modeling makes it possible to determine the optimal parameters that could be used for developing tomographic systems [36, 37].

Wavelength (or pulse width and frequency bandwidth) of the ultrasonic radiation is an important parameter. Ultrasonic tomography equipment for early breast cancer diagnosis should detect inhomogeneities of about 3 mm in size and distinguish them from the surrounding tissues. Sound speed inside an inhomogeneity should be determined within several percents, since in soft tissues sound speed in the tumor and that in the healthy tissue differ only slightly — by less than 10%. There are two main factors that influence the choice of the ultrasonic radiation wavelength. First, it is ultrasound absorption in tissues, which increases as the frequency increases. Despite the fact that high frequencies in the 1 – 10 MHz range are widely used in ultrasound equipment, the use of such high frequencies in the tomographic scheme is problematic, since tomographic reconstruction requires high accuracy of measurements, and too weak signal does not allow this. Secondly, increasing the frequency results in increasing the complexity of equipment, such as the number of detectors, quality of the signal processing hardware, etc.

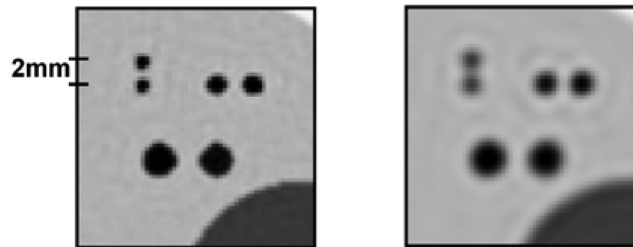
Let's show that it is possible to achieve the resolution of about 3 mm using the wavelength of about 5 mm. We will illustrate this fact by the following numerical simulations. In the 3D numerical experiment, 24 source were used, located in planes  $z=h_0$  and  $z=h_1$  as shown on fig. 13. The detectors were located on all the faces of the cubic computational domain; the inter-detector distance is 2 mm. The waveform of the sounding pulse is shown in fig. 8. The calculations were made for pulses with width  $\lambda=5$  mm and  $\lambda=10$  mm.

Fig. 16 shows cross-sections of the reconstructed 3D sound speed image for initial pulses with wavelength of  $\lambda=5$  mm and 10 mm. Fig. 17 shows enlarged fragments of the images. It can be seen that at  $\lambda=10$  mm, the quality of restored 2 mm details is not satisfactory. Therefore, the optimal wavelength would be  $\lambda \approx 5$  mm. Note that such a high spatial resolution is obtained even having a very low contrast of the test object, sound speed variation in which does not exceed 10%.

The quality of reconstructed tomographic images depends on the accuracy of the input data. The error level of the input data depends on both random factors, such as crosstalk, equipment noise, etc., and on the setup, such as sampling frequency and the number of digitization levels.



**Figure 16.** The images reconstructed using 5mm and 10mm initial pulses



**Figure 17.** Magnified images reconstructed using 5mm (left) and 10mm (right) initial pulses

Let's define, with the help of mathematical modeling, the allowable error levels of the input data for ultrasound tomography. The level of input data error  $\delta$  is measured relative to the maximum amplitude of the signal at the detectors:  $A = \max(U(\mathbf{s},t)) - \min(U(\mathbf{s},t))$ , which is assumed as 100%.

Fig. 18 shows cross-sections of the 3D images reconstructed using perturbed data. The error levels of  $0.015 \cdot A$  (1.5%) and  $0.05 \cdot A$  (5%) were simulated by adding pseudo-random noise to the input data  $U(\mathbf{s},t)$  at the sampling rate of 10 MHz. The sources were located according to fig. 13, in two planes  $z=h_0$  and  $z=h_1$ , the detectors were located on all the faces of the cube with 2.5 mm spacing between the adjacent detectors.

From the fig. 18 it can be seen that with the error level of 1.5%, it is still possible to obtain high-resolution images. With the error of 5%, the restored image still contains some information about the small inclusions present in the numerical phantom, but the image quality deteriorates significantly.

Comparison of the images (fig. 19) shows that precision of the input data is important, the quality of image reconstruction improves as the error decreases, and the tomographic instruments are intended to make this error as small as possible. Thus, the design should take into account the overall level of input data error not exceeding 3 to 5%.

## 4. Discussion and conclusion

1. The article discusses various diagnostic tasks where the tomographic approach is used. The tomographic approach involves studying the object from various points of view. Tomographic methods can significantly increase the resolution of both medical and industrial di-

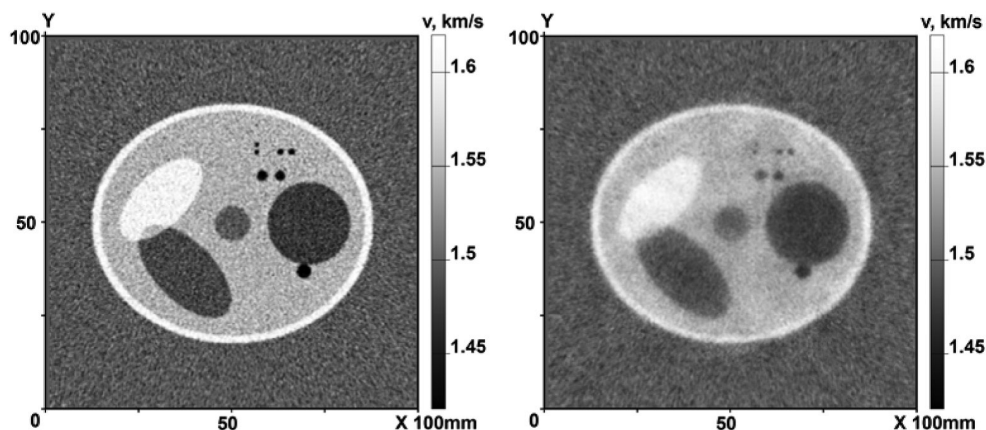


**Figure 18.** Cross-section in the  $Z=66$  mm plane obtained with the error levels of 1.5% (left) and 5% (right)

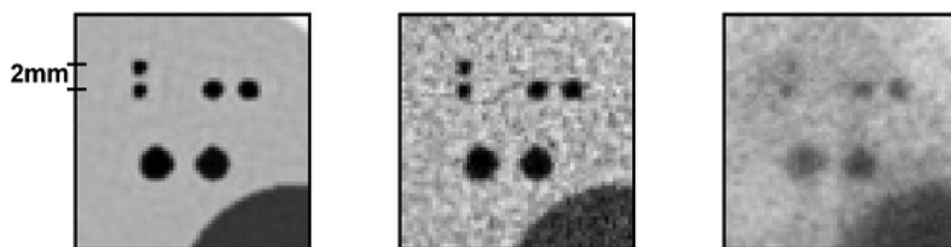


**Figure 19.** Magnified images obtained without error (on the left) with the error level of 1.5% (center) and 5% (right)

agnostic systems. One of the variants of tomographic imaging is the method of synthesized aperture, where the object is examined only from a narrow angular range. However, for some tasks, like radar surveys, this approach makes it possible to increase the resolution of the obtained images by hundreds of times. From the mathematical point of view, most of the tasks of synthetic aperture data interpretation can be reduced to solving linear problems. Using SAR in on-line mode involves processing huge amounts of data in real time, which requires the use of graphics accelerators.

Unfortunately, from the applications point of view, linear models of synthesized aperture are effective only for a limited class of applications. An example of such tasks may be studying the Earth's surface from a spacecraft in the centimeter wavelength range. An important limitation of the model is the fact that the medium between the radiation source and the studied object should be homogeneous. For reconstructing the internal structure of objects, the use of the synthetic aperture method is limited.

2. Tomographic examination, where the object can be studied using numerous source and detector positions, ideally — viewed under all angles (full-range tomography), allows precise reconstruction of the internal structure of examined objects. X-ray tomographs are used most widely; they are used both in medicine and in non-destructive testing. A modern trend in the medicine is limiting the use of harmful ionizing radiation. From this point of view, development of methods of ultrasonic tomography is promising. The most relevant medical application is differential diagnosis of breast cancer.

3. Unlike X-ray tomography, inverse problems of wave tomography are nonlinear and three-dimensional. This article describes modern methods of solving inverse problems of wave tomography as coefficient inverse problems for hyperbolic differential equations. Such problems cannot be solved without using supercomputers. This article describes numerical simulations that show efficiency of algorithms for solving 2D and 3D coefficient inverse problems arising in ultrasound tomography. Both CPU and GPU processors were used to solve the test problems.

4. The three-dimensional model is the most adequate to the reality. The developed algorithms are focused on using GPU clusters, which are most suitable for solving inverse problems in 3D formulation. The performance-comparable systems based on general-purpose processors have 5–10 times higher cost than GPU-based systems. The FDTD method employed can be efficiently parallelized on SIMD/SPMD architectures; however, this method is memory-intensive and requires high memory bandwidth. Numerical simulations have been performed using NVidia Tesla X2070, NVidia GeForce GTX 460 and NVidia GeForce GTX Titan graphics cards. The time spent for calculating the gradient for a single ultrasound source in a three-dimensional inverse problem for NVidia Tesla X2070 and GTX Titan was  $\sim 45$  seconds, therefore the complete image reconstruction ( $\sim 120$  gradient descent iterations) takes about 2 hours. The computation time was twice as long for the entry-level NVidia GeForce GTX 460 graphics card. Calculations for each source can be performed independently; therefore, the task can be easily parallelized to a number of devices corresponding to the number of sources (possibly 25–40 in an actual tomographic setup), so the inverse problem can be solved for all the sources in about 2 hours using such GPU cluster. Almost all the data involved in the process were placed in the onboard GPU memory, the required volume of which is 3 GB for the image size of  $400^3$ . If larger image dimensions are required, computations for each source may be parallelized to 2–4 GPU devices to maintain acceptable computation time.

5. The technology of tomographic image reconstruction by solving coefficient inverse problems may be implemented at present time in tomographic facilities, although it is at the limit of the capabilities of modern technology. At present, supercomputers are just starting to be used for medical research. However, the rate of computer technology development has enormous potential for development of new generation diagnostic systems based on wave tomography. In particular, in 2016, launch of NVidia Pascal or AMD Polaris devices based on HBM (High Bandwidth Memory) architecture has been announced, which allows achieving the performance of up to 1 TB/sec, which would speed up the calculations by 3–4 times compared to the currently available graphics cards, simultaneously reducing power consumption. The use of such computing devices will make it possible to build computing systems that could be widely used in medical ultrasonic tomography facilities.

6. From the mathematical point of view, an important parameter for solving an inverse problem is the error of the obtained approximate solution to the inverse problem. It is a strictly mathematical concept. Let  $\bar{c}(\mathbf{r})$  be the exact solution for the given input data  $u=U$ . Let the input information be specified with error  $\delta$ , that is,  $u_\delta$  is set so that  $\|u_\delta - u\| \leq \delta$ . Following the basics of the regularizing algorithms theory, the concept of an algorithm R for the approximate solution  $R=R(u_\delta, \delta)$  is introduced [43]. The algorithm allows finding the approximate solution of the problem  $c_\delta=R(u_\delta, \delta)$ , according to the given values of  $\delta$  and  $u_\delta$ . The algorithm is called regularizing if  $c_\delta \rightarrow \bar{c}$  if  $\delta \rightarrow 0$  [38, 39]. The value  $\varepsilon(\delta) = \|c_\delta - \bar{c}\|$  is the error of the approximate solution. Let us note right away that in fact the error of the approximate solution is not only the function of  $\delta$ , but it also depends on the exact solution  $\bar{c}$ , that is,

$\|c_\delta - \bar{c}\| = \varepsilon(\delta, \bar{c})$ . Thus, the error of the approximate solution can be defined only at each fixed point  $c = \bar{c}$ . Naturally, the error of the approximate solution is different for different points  $\bar{c}$ . When solving the model problem,  $\bar{c}$  is fixed, and the model problems demonstrate how the approximate solution is close to exact solution  $\bar{c}$ . With  $\delta \rightarrow 0$ , the approximate solution tends to the exact solution of the problem, which corresponds to the infinitely high resolution that can be obtained with the error tending to zero. The developed algorithms have all the characteristics listed above. The possibility to approximate the exact solution of the problem arbitrarily precise, if  $\delta \rightarrow 0$  means that it is possible to achieve arbitrarily high resolving power, provided that the error level  $\delta$  is sufficiently small.

The study of the error  $\varepsilon(\delta, c)$  for a fixed level  $\delta$  is most interesting. For solving the model problems, it is necessary to choose the test object (numerical phantom) that is as close to reality as possible. If  $\delta$  and  $\bar{c}$  are fixed, the magnitude of error  $\varepsilon(\delta, \bar{c})$  depends on the scheme of the experiment, the number of the sources and their positions, the number of detectors and their size, the number of grid points, and on other parameters. The task of mathematical modeling is choosing the optimum parameters of ultrasonic equipment, which requires performing many numerical simulations with various parameters of the tomographic setup. When designing ultrasonic tomography equipment, mathematical modeling makes it possible to save not only money, but development time as well. The arising mathematical problems cannot be solved without using supercomputers.

*This work was supported by the Russian Foundation for Basic Research (Project No. 14-07-00078-a). The reported study was supported by the Supercomputing Center of Lomonosov Moscow State University [40].*

1. Glide-Hurst C.K., Duric N., Littrup P. Volumetric breast density evaluation from ultrasound tomography images // Medical Physics. 2008. 35. 3988-3997. DOI: 10.1118/1.2964092.
2. Matej S., Fessler J.A., Kazantsev I.G. Iterative tomographic image reconstruction using fourier-based forward and back-projectors IEEE Transactions on Medical Imaging. 2004. Vol. 23. p. 401. DOI: 10.1109/NSSMIC.2002.1239651.
3. Bazulin A.E., Bazulin E.G., Vopilkin A.K., Kokolev S.A., Romashkin S.V., Tikhonov D.S. Application of 3D coherent processing in ultrasonic testing // Russian journal of nondestructive testing, Vol. 50, No. 2, 2014. pp. 92-108. DOI: 10.1134/S1061830914020028
4. Levin G.G., Vishnyakov G.N., Minaev V.L., Latushko M.I., Pickalov V.V., Belyakov V.K., Sukhenko E.P., Demyanenko A.V. Shearing interference microscopy for tomography of living cells // Proceedings of SPIE, Vol. 9536, 2015. pp. 95360G. doi: 10.1117/12.2183717
5. Glinskii B.M., Sobisevich A.L., Khairtadinov M.S. Experience of vibroseismic sounding of complex geological structures (with the Shugo mud volcano as an example) Doklady earth sciences, 2007, Vol. 413, No. 3. pp.397-401. DOI: 10.1134/S1028334X07030178
6. Digisens 3D tomography software solutions. <http://www.digisens3d.com/>
7. Jia X., Yan H., Cervino L., Folkerts M., Jiang S.B. A GPU tool for efficient, accurate, and realistic simulation of cone beam CT projections // Med Phys. 2012 Dec;39 (12):7368-78. doi: 10.1118/1.4766436. DOI: 10.1118/1.4766436.
8. Wiskin J., Borup D., Johnson S., Berggren M., Robinson D., Smith J., Chen J., Parisky Y., Klock J. Inverse scattering and refraction corrected reflection for breast cancer imaging // Proc. of SPIE Vol. 7629 76290K-1. doi: 10.1117/12.844910.
9. Gemmeke H., Menshikov A., Tchernikovski D., Berger L., Gobel G., Birk M., Zapf M. and Ruitter N. V. 2010 Hardware setup for the next generation of 3D ultrasound computer

- tomography Nuclear Science Symposium Conference Record (NSS/MIC) IEEE pp 2449-54. DOI: 10.1109/NSSMIC.2010.5874228
10. Burov V.A., Zotov D.I., Rumyantseva O.D. Reconstruction of spatial distributions of sound velocity and absorption in soft biological tissues using model ultrasonic tomographic data // *Acoustical Physics*, 2014, V 60, No. 4, pp. 479-491. DOI: 10.1134/S1063771014040022
  11. Kak A, Slaney M. Principles of computerized tomographic imaging. SIAM, 2001.
  12. Radon, J.; Parks, P.C. (translator) (1986), On the determination of functions from their integral values along certain manifolds, *IEEE Transactions on Medical Imaging* 5 (4): 170–176, doi:10.1109/TMI.1986.4307775, PMID 18244009.
  13. Schmidt S., Gade-Nielsen N.F., Hstergaard M., Dammann B., Kazantsev I.G., High Resolution Orientation Distribution Function // *Materials Science Forum*, 2012, Vols. 702-703, pp. 536-539.
  14. Barber B. C. Theory of digital imaging from orbital synthetic aperture radar // *IJRS*, 11, 1983.
  15. Elachi C., Bicknell T., Jordan R. L., Chialin Wu. Spaceborne synthetic-aperture imaging radars: Applications, techniques, and technology // *Proceedings of the IEEE* 1982, Vol 70, Issue: 10 pp.1174 - 1209.
  16. Kretzek E., Ruiter N.V. GPU based 3D SAFT reconstruction including phase aberration // *Proc. SPIE 9040, Medical Imaging 2014: Ultrasonic Imaging and Tomography*, 90400W (March 20, 2014); doi:10.1117/12.2042669
  17. Tikhonov A.N., Goncharskii A.V., Matvienko A.N., Romanov S.Y., Shchetinin V.G., Chubarov I.N., Markachev S.I., Grishko M.I., Ksenofontov E.A. Problems in the digital reconstruction of synthetic-aperture radar images // *Soviet Physics Doklady*, 1992, Vol. 37, pp. 79.
  18. Rubin G., Berger D., Sager E. GPU Acceleration of SAR/ISAR Imaging Algorithms // *Antenna Measurement Techniques Association Symposium 2010 (AMTA 2010)*, Proceedings of a meeting held 10-15 October 2010, Atlanta, Georgia, USA. A10-0059. pp. 430-435.
  19. Maddikonda S.S., Shanmugha Sundaram G.A. SAR image processing using GPU // *Communications and Signal Processing (ICCSP)*, 2014 International Conference on. pp. 448 – 452. DOI: 10.1109/ICCSP.2014.6949881
  20. Bakushinsky A.B., Goncharsky A.V. Ill-posed problems. Theory and applications. Dordrecht: Kluwer, 1994.
  21. Goncharskii A.V., Romanov S.Y. On a three-dimensional diagnostics problem in the wave Approximation // *Computational Mathematics and Mathematical Physics* 2000;40:1308–1311. DOI: 10.3103/S0278641910010012
  22. Goncharskii A.V., Ovchinnikov S.L., Romanov S.Y.. On the one problem of wave diagnostics // *Moscow University Computational Mathematics and Cybernetics* 2010;34:1–7. DOI: 10.3103/S0278641910010012
  23. Ovchinnikov S.L., Romanov S.Yu. Organization of parallel computations when solving the inverse problem of wave diagnostics // *Vychisl. Metody Programm.* 2008. Vol.9. N 2. pp.338-345. (in Russian).
  24. Goncharskii A.V., Romanov S.Yu. Two Approaches to the Solution of Coefficient Inverse Problems for Wave Equations // *Computational Mathematics and Mathematical Physics*. 2012, Vol. 52, No. 2, pp. 245–251.

25. Glover G.H. Computerized time-of-flight ultrasonic tomography for breast examination // *Ultrasound in Medicine & Biology* Vol, 3, No. 2–3, 1977, pp. 117-127. doi:10.1016/0301-5629(77)90064-3
26. Toward real-time bent-ray breast ultrasound tomography using GPUs// *Proceedings of SPIE - The international society for optical engineering* 9040 february 2014. DOI: 10.1117/12.2043127
27. Natterer F. Possibilities and limitations of time domain wave equation imaging. *Contemporary Mathematics* 2011;559:151–162.
28. Beilina L. and Klibanov M.V. 2012 *Approximate Global Convergence and Adaptivity for Coefficient Inverse Problems* (New York: Springer).
29. Goncharsky A.V., Romanov S.Y. Supercomputer technologies in inverse problems of ultrasound tomography // *Inverse Problems*. 2013, Vol. 29, No. 7. 075004. DOI: 10.1088/0266-5611/29/7/075004.
30. Goncharsky A.V., Romanov S.Y. Inverse problems of ultrasound tomography in models with attenuation. *Phys Med Biol*. 2014;59:1979–2004. DOI: 10.1088/0031-9155/59/8/1979
31. Goncharsky A.V., Romanov S.Y., Seryozhnikov S.Y. Inverse problems of 3D ultrasonic tomography with complete and incomplete range data. *Wave motion* 2014;51:389–404. DOI: 10.1016/j.wavemoti.2013.10.001
32. Huang L., Quan Y. Sound-speed tomography using first-arrival transmission ultrasound for a ring array // *Proc. SPIE Medical Imaging*. 2007. 6513. doi: 10.1117/12.709647.
33. Roy O., Jovanovic I., Hormati A., Parhizkar R., Vetterli M. Sound Speed Estimation Using Wave-based Ultrasound Tomography: Theory and GPU Implementation // *Proc. SPIE 7629, Medical Imaging 2010: Ultrasonic Imaging, Tomography, and Therapy*. 2010. 76290J. doi:10.1117/12.844691.
34. Varadan V.V., Ma Y., Varadan V.K., Lakhtakia A. Scattering of waves by spheres and cylinders // in: *Field representations and Introduction to Scattering*. (North-Holland), Amsterdam. 1991. 211-324.
35. Lavarello R.J., Oelze M.L. Tomographic Reconstruction of Three-Dimensional Volumes Using the Distorted Born Iterative Method // *IEEE Trans. Med. Imaging*. 2009. 28. 1643-1653. DOI: 10.1109/TMI.2009.2026274.
36. Goncharsky A.V., Romanov S.Yu., and Seryozhnikov S.Yu. Problems of limited-data wave tomography // *Vychisl. Metody Programm.* 2014 (15), 274–285 (in Russian).
37. Goncharsky A.V., Romanov S.Y., Seryozhnikov S.Y. A computer simulation study of soft tissue characterization using low-frequency ultrasonic tomography // *Ultrasonics*, 2016. V. 67, pp. 136–150. DOI: 10.1016/j.ultras.2016.01.008.
38. Tikhonov A.N. The solution of ill-posed problems and the regularization method, *DAN SSSR* 151: 3 (1963), pp.501-504 (in Russian)
39. Tikhonov A.N., Goncharsky A.V., Stepanov V.V., Yagola A.G. *Numerical Methods for the Solution of Ill-Posed Problems*. Kluwer acad.publ. Dordrecht/Boston/London 1995. ISBN 0-7923-3583-X
40. Sadovnichy V., Tikhonravov A., Voevodin Vl., and Opanasenko V. "Lomonosov": Supercomputing at Moscow State University. In *Contemporary High Performance Computing: From Petascale toward Exascale* (Chapman & Hall/CRC Computational Science), pp.283-307, Boca Raton, USA, CRC Press, 2013.